ACS APPLIED MATERIALS & INTERFACES

Research Article

www.acsami.org

$LiMnBO_3$ Nanobeads As an Innovative Anode Material for High Power Lithium Ion Capacitor Applications

Karthikeyan Kaliyappan,*[†,‡] Samuthirapandiyan Amaresh,[†] and Yun-Sung Lee*[†]

[†]Faculty of Applied Chemical Engineering, Chonnam National University, Gwang-ju 500-757, Korea

[‡]Department of Mechanical and Materials Engineering, The University of Western Ontario, London, Ontario, N6A 5B9, Canada

Supporting Information

ABSTRACT: A novel approach was made to fabricate lithium ion hybrid capacitor (Li-HC) having $LiMnBO_3$ nanobead (LMB-NB) anode and polyaniline nanofiber (PANI) cathode in 1 M $LiPF_6$ organic electrolyte. LMB-NB and PANI nanofibers were synthesized using urea assisted microwave-solvothermal method and chemical polymerization process, respectively. The PANI/LMB-NB cell showed improved electrochemical capacitive behavior as compared to activated carbon (AC)/LMB-NB cell due to the characteristic conductivity and the morphological feature of PANI as well as LMB-NB electrodes. A discharge capacitance (DC_{cell}) of ~125 F g^{-1} was obtained at a current density of 1 A g^{-1} between the potential range 0 and 3 V for PANI/LMB-NB cell, while AC/LMB-NB cell delivered only 77 F g^{-1} at the same current density. Moreover, PANI/LMB-NB cell exhibited excellent rate performance with the DC_{cell} of about 55 F g^{-1} at 2.25 A g^{-1} and still retained 94% of the initial value after 30 000 charge–discharge cycles. In addition, maximum energy and power densities of 42 Wh kg^{-1} and 5350 W kg^{-1}, respectively, were achieved from PANI/LMB-NB cell. The obtained DC_{cell}, energy, and power densities along with prolonged cyclic life for PANI/LMB-NB cell are some of the best ever reported values for Li-HC as compared to the cells constructed with various lithium intercalating materials.

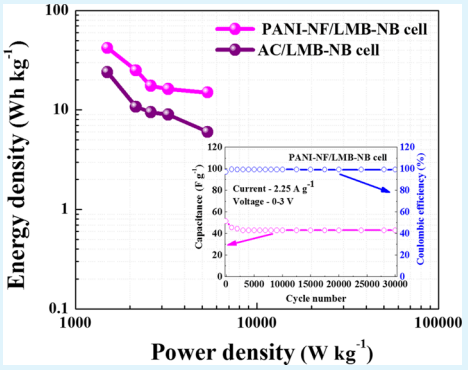

KEYWORDS: *lithium ion capacitor, PANI, $LiMnBO_3$, energy density, conducting polymer*

INTRODUCTION

Recently, a new class of energy storage system, the so-called "lithium ion hybrid capacitors" (Li-HCs), is drawing much attention due to the characteristic ability to overcome the energy and power density limitation of conventional electrochemical double layer capacitor (EDLC) and nonaqueous batteries, respectively.[1] The Li-HC cells can be fabricated using a Li-insertion material as energy source and a capacitive material as power source.[2] The enhancement in specific energy and cell voltage of Li-HC along with prolonged cycle life resulted from the construction of Li-HC with two different kinds of electrodes involving two different storage mechanisms. As a consequence, the Li-HC delivered improved energy density (up to 4–5 times higher as compared to those of conventional EDLC). Therefore, Li-HCs are being considered as an alternative energy storage device for zero-emission transportation vehicles.[2−4]

Because the electrode materials played a critical role in improving storage properties of Li-HC, the selection of energy source electrode with high redox potential was important for increasing the cell voltage as well as the energy and power densities. There are several one-dimensional metal oxides, such as NiO, MnO_2, and Co_3O_4, etc., reported for Li-HC applications. Yet, the low redox potential and metal dissolution restricted these materials to be applied for high performance Li-HCs.[5−7] Lithium intercalation materials as energy sources are considered as the best candidates for Li-HCs due to their high theoretical capacity, high working voltage, and energy density.[8,9] Initially, $Li_4Ti_5O_{12}$ was utilized as negative electrode in nonaqueous hybrid system.[10] Wang et al. presented the Li-HCs with $LiMn_2O_4$ and $LiCo_{1/3}Ni_{1/3}Mn_{1/3}O_2$ as cathode and activated carbon (AC) anode in an aqueous electrolyte.[11,12] Of late, olivine-type materials such as $LiCoPO_4$ and $LiFePO_4$ were successfully adopted as cathode material for Li-HC application.[13,14] Among them, Mn-based layered or spinel lithium intercalation materials and their derivatives could be considered as suitable candidate for Li-HCs because of the low toxicity and natural abundance. However, all of these materials showed continuous capacitance fading during the electrochemical charge–discharge (C–DC) process due to the dissolution of active species, affecting their long-term cyclability and rate performance, limiting the applicability for practical use. Also, the thermal stability of the aforementioned energy source electrodes is also questionable. To circumvent these issues, we have successfully adopted a new family of lithium insertion hosts, orthosilicates (Li_2MSiO_4, M = Fe or Mn) and fluoro-oxyanion (Li_2CoPO_4F) as potential energy source materials for Li-HCs along with (AC) as anode with superior rate

Received: March 30, 2014
Accepted: June 9, 2014
Published: June 9, 2014

 © 2014 American Chemical Society

performance and high energy densities.[15−17] Despite delivering enhanced energy and power densities with prolonged cycling life at high rate, the difficulty in obtaining phase pure orthosilicates and fluorophosphates materials makes them inappropriate for high power applications such as electrical vehicles (EVs) and hybrid electrical vehicles (HEVs).

Consequently, finding new energy source materials with good thermal stability and high safety is the major challenge for the advancement of Li-HC in the future. In recent times, lithium metal borates ($LiMBO_3$, M = Mn, Fe, Co) have been reported as promising alternative cathodes for lithium-ion battery (LIB) due to their high theoretical capacity (>220 mAh g^{-1}), thermal stability, comparable density, electrochemical stability due to small volume changes, natural abundance, and environmentally benign nature.[18] Moreover, the BO_3^{3-} group also has lower weight than the PO_4^{3-} group metal borates, and thereby could be a better substitute for phosphates.[18,19] Borates have also exhibited higher operating voltage and enhanced structural stability by keeping the benefit of a networking anion group, but possessing low electrical conductivity similar to that of the olivine framework. Legagneura et al. first showed the possibility of utilizing $LiFeBO_3$ and $LiMnBO_3$ as positive electrode for LIB with low electrochemical activity.[18] Generally, $LiMnBO_3$ (LMB) exists in two polymorphs, which is either hexagonal (h-LMB) or monoclinic (m-LMB) phases, and has higher energy density along with high redox voltage (4.1 V/3.7 V) as compared to $LiFeBO_3$.[20,21] In the case of m-LMB, the first electrochemical activity was recorded by Kim et al. with a discharge capacity of 100 mA g^{-1}.[20] On the other hand, h-LMB delivered low charge/discharge characteristics between the voltage range of 4.8−1.25 V. Nevertheless, LMB also suffered from low inherent electronic conductivity, which required extensive studies to improve their electrochemical performance. Because LMB still required several valid attempts and strategies before being successfully adopted as an alternative for $LiCoO_2$ in LIB applications, their adjustable voltage platform characteristics motivated us to utilize them as energy source material for Li-HCs. It is well-known that surface morphology played an important role in enhancing the energy storage behavior. Utilization of nano sized active materials with high surface area for Li-HCs, reducing the pathway for Li-ion diffusion through the size effect, and hence enhanced rate capability could be achieved. Moreover, forming a highly conductive network between the nano-LMBs is also an effective way to improve its inherent conductive nature as well as the electrochemical reaction kinetics. In this regard, we are presenting LMB nanobeads as a cheap and eco-friendly energy source for Li-HC application.

On the other hand, carbonaceous materials are a widely used electrode material for Li-HCs.[15−17,22] Lately, prelithiated graphitic anode (G) is being utilized for commercialized Li-HC application along with AC cathode in G/AC configuration.[23] Unfortunately, the tedious prelithiation process and the formation of solid electrolyte interface during cycling process hindered the mass production of the graphitic anodes for Li-HC applications. Although activated carbon is a promising candidate for such applications with desirable features like low cost, chemical, and thermal stability, the low bulk density and poor charge storage capability restricted them to be applied in high energy density applications. Additionally, the risk of high surface area Li plating during high current cycling leads to the search of alternatives for AC with both higher capacitance and more positive intercalation voltage.[23] Later, various transition metal oxides (TMO) were employed as negative electrode for Li-HCs along with improved energy density value.[5] Unfortunately, dissolution of TMO during electrochemical cycling is a major challenge for achieving high performance Li-HCs with prolonged cycle life.

Of late, electrochemically conducting polymers (CPs) are being considered as the electrode material for Li-HCs because of the inherent conductivity and high specific capacitance values.[24] Utilizing p- and n-dopable polymers in Li-HCs is the best way to enhance energy and power densities of a single cell, which resulted from their high working voltage.[25] Although the pseudocapacitance properties of CPs and their derivatives had been extensively studied, there are limited reports available on fabricating Li-HC using CP as power source material.[5] Pasquier et al. reported $Li_4Ti_5O_{12}$/poly(methyl)thiophene cell with a specific energy of 10 Wh kg^{-1}.[26] Park et al. and Torres et al. presented asymmetric hybrid capacitor with AC and polyaniline (PANI) electrodes.[27,28] Despite exhibiting better cycling performance and low cost properties, low specific energy of those systems limited them to be applied in practical application. Latter, we have reported a $Li(Mn_{1/3}Ni_{1/3}Fe_{1/3})O_2$−PANI hybrid composite electrode as a high performance energy source for Li-HC application along with AC anode.[29] Among the CPs reported, *p*-dopable PANI as capacitive electrode has certain advantages such as high electrical conductivity in its oxidized/protonated form, higher chemical stability, stable electrochemical behavior, and better acid/base properties.[24,27] Furthermore, PANI nano fiber as electrode material for supercapacitors is known to exhibit high pseudocapacitance value along with excellent columbic efficiency.[28] Considering the advantages of nano sized m-LMB and PANI, an attempt has been made to study the capacitive performance of Li-HC consisting of m-LMB anode and PANI electrodes in standard organic electrolyte. Better electrochemical characteristics could be expected from PANI/m-LMB cell due to the intercalation/deintercalation mechanism of m-LMB and highly reversible doping−dedoping process of PANI.[27] In addition, AC/m-LMB cell was also fabricated, and the electrochemical performances of both of the cells were simultaneously compared using cyclic voltammetry (CV), charge−discharge studies (C/D), and electrochemical impedance spectroscopy (EIS).

EXPERIMENTAL SECTION

AC with a surface area of 1600 m^2 g^{-1} was received and used without any further modification. PANI was prepared by chemical polymerization route in which the polymerization process was initiated by the slower addition of ammonium persulfate ($(NH_4)_2S_2O_8$) as oxidant into aniline in 1 M HCl solution. A detailed description of polymerization process could be found in our previous paper.[29]

The $LiMnBO_3$ nanobeads (LMB-NB) were synthesized using microwave irradiation-solvothermal method with urea as surfactant. Initially, lithium nitrate (Sigma-Aldrich, 99%), manganese nitrate (wako, 99.8%), and boric acid (Sigma-Aldrich, 99.9%) with the molar ratio of 1.05:1:1, respectively, were dissolved in 100 mL of distilled water. Next, the appropriate amount of urea was added into the above solution and stirred for 90 min. The molar ratio of metal ions to urea was fixed at 1:10. The final solution then was irradiated in a household microwave oven (700 W, Daewoo, Korea) for 20 min. After being cooled, the resultant was continuously washed with distilled water followed by absolute ethanol and dried at 80 °C for 24 h. Finally, carbon-coated LMB-NB with high crystallinity was obtained by firing the dried product at 650 °C for 7 h in argon atmosphere.

The phase analysis of LMB-NB was done using X-ray diffraction measurements (XRD, Rint 1000, Rigaku, Japan) equipped with Cu Kα

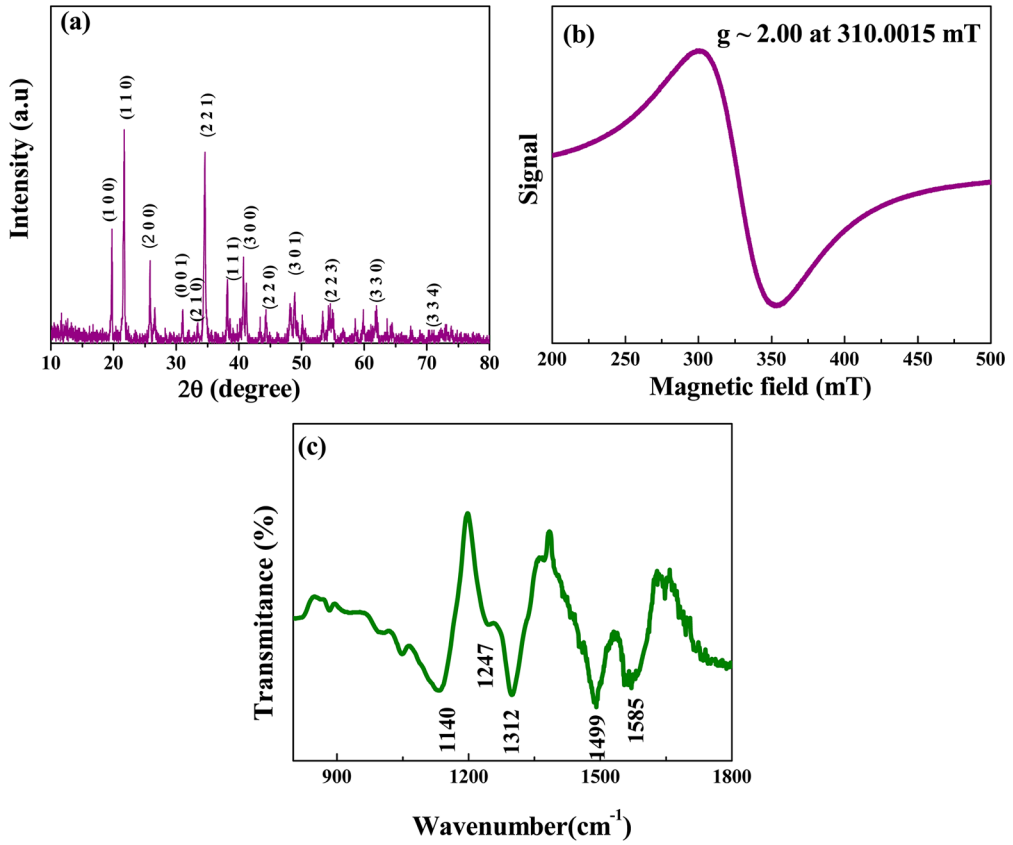

Figure 1. (a) XRD, (b) EPR spectrum of LMB-NB prepared at 650 °C for 7 h under argon atmosphere. (c) FT-IR pattern of PANI prepared using chemical polymerization technique at ambient temperature.

as the radiation source. The formation of PANI was confirmed by Fourier transform infrared (FT-IR) spectroscopy on an IRPrestige-21 spectrometer, Japan. Brunauer–Emmett–Teller (BET) surface area analysis was performed using an ASAP 2010 surface analyzer (Micromeritics, U.S.). The morphological feature of the prepared samples was examined by a field emission transmission electron microscope (TEM, Tecnai-F20, Philips, Netherland). The Raman spectrum was done in a micro-Raman spectrometer (LabRam HR 800, France) with holographic gratings.

The electrochemical analysis of the half cells was conducted using a 2032 coin cell configuration in which PANI or LMB-NB or AC served as working electrode and lithium foil acted as counter electrode. The electrodes were prepared by pressing a slurry of 80% active material (PANI or LMB-NB or AC), 10% ketzen black (KB) as conductive additive, and 10% Teflonized acetylene black (TAB) binder on a 200 mm^2 nickel mesh and dried at 160 °C for 4 h in an oven. The half cells were fabricated in an argon-filled glovebox by sandwiching a working electrode and lithium negative electrode separated by a separator (Celgard 3401) with 1 M $LiPF_6$ dissolved in a mixture of ethylene carbonate (EC) and dimethyl carbonate (DMC) (1:1 v/v, Soulbrain Co., Ltd., Korea) as electrolyte. The same procedure was also used for PANI/LMB-NB construction where LMB-NB and PANI were used as anode and cathode, respectively, after optimizing the mass ratio of the electrode materials. For comparison, AC/LMB-NB was also fabricated using the above-mentioned method. The cyclic voltammetry (CV) and the electrochemical impedance spectroscopy (EIS) measurements were done using an electrochemical analyzer (SP-150, Bio-Logic, France). The charge/discharge (C–DC) characteristics of the assembled Li-HC cells were performed at different current rates between 0 and 3 V using a cycle tester (WBCS 3000, Won-A-Tech, Korea).

RESULTS AND DISCUSSION

The XRD pattern of LMB-NB prepared at 650 °C for 7 h was presented in Figure 1a. It is well-known that the structure of LMB-NB is isostructural to hexagonal $LiCdBO_3$, which was constructed from planar BO_3 groups, LiO_4 in the tetrahedral sites, and MnO_5 square pyramids.[30] In addition, all of the peaks could be indexed on the basis of the monoclinic phase with *C*2/*c* space group according to the JCPDS card no. 83-2342.[21,30] Moreover, well-developed and narrow XRD peaks revealed good crystalline nature of LMB-NB powders. It is well-known that LMB has two isotopes of hexagonal and monoclinic structures, and the formation of these phases was mainly influenced by the calcination temperature. In the present investigation, LMB-NB with monoclinic structure was synthesized at 650 °C, exhibiting better electrochemical properties than that of hexagonal structure.[20] The lattice parameters a = 5.192 Å, b = 8.944 Å, and c = 10.328 Å were observed to be in good agreement with the other research results for m-LMB.[21] In addition, the average crystallite size of powders grown by microwave irradiation method was found to be ~40 nm using Scherrer's formula.[16] The presence of Mn^{2+} in LMB-NB was confirmed using electron paramagnetic resonance (EPR), and the corresponding spectrum was presented in Figure 1b. As seen from the spectrum, EPR of LMB-NB showed a single broad line centered at 310.025 mT $g \approx 2.00$, indicating the existence of manganese ions in 2^+ state.[31]

The FT-IR spectrum of PANI nanofibers was illustrated in Figure 1c, demonstrating successful oxidation of aniline monomer by APS oxidant in 1 M HCl solvent. The peaks observed at 1585 and 1499 cm^{-1} represented the stretching

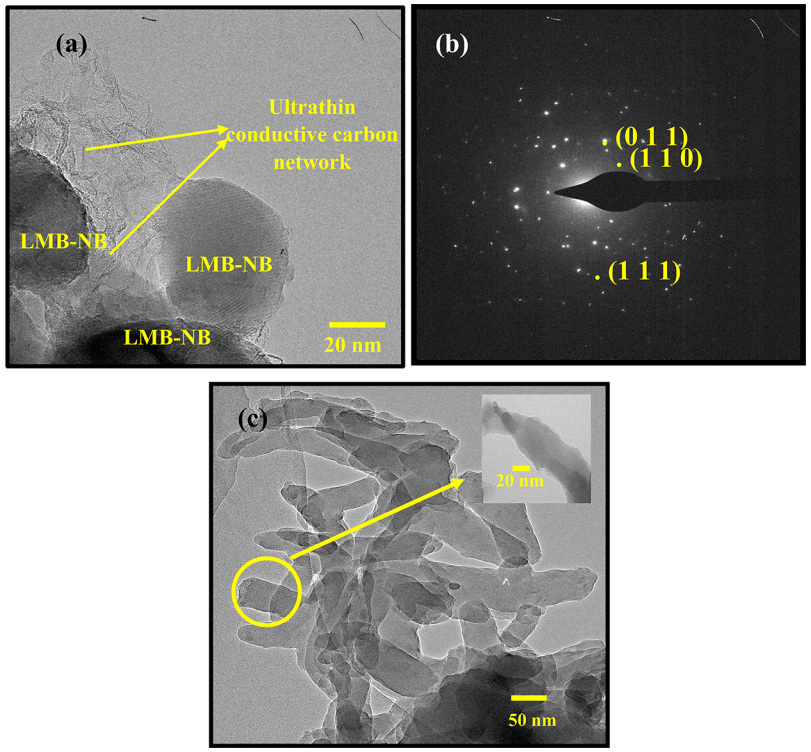

Figure 2. (a) TEM, (b) SAED pattern of LMB-NB. Recorded diffraction rings are indexed with corresponding Miller indices and (c) TEM image of PANI nanofibers.

vibration of quinoid and benzenoid, respectively, which indicated the presence of its emeraldine salt.[32] The characteristic peak observed at 1140 cm^{-1} could be assigned to the measurement of the electrons' delocalization, that is, electronic conductivity.[29] The strong bonds at ∼1312 and ∼1247 cm^{-1} were attributed to Ph−N and C−NH^+ stretching vibrations, respectively.[29,32]

The morphological features of LMB-NB and PANI nanofibers were presented in Figure 2. As seen from Figure 2a, the LMB-NBs consisted of a large number of nanobeads of about 30−40 nm in diameter, which was in good agreement with the size obtained from XRD data. In addition, LMB-NBs were concentric, uniform in size, and connected with each other by amorphous carbon network that resulted in the formation of weblike morphology. The oxygen present in urea readily oxidized the amorphous carbon in situ, which is responsible for getting the nanobeads of uniform diameter. This morphological feature of LMB-NBs allowed one to accommodate more electrolytes within the structure, which provided more active sites and flexible structure and thereby eliminated the volume changes during the electrochemical cycling process. Moreover, highly interconnected LMB-NBs increase the electrode−electrolyte interfacial area by providing a path for better lithium ion diffusion and alleviated the intrinsic nature of LMB-NB electrodes. It is well-known that the electrode material with high number of reaction sites, uniform particles with homogeneous size distribution, and stable structure are essential parameters for improving the C−DC capability of Li-HCs at high current rate.[17,29]

The presence of carbon was confirmed using EDX, and the corresponding dot mapping was shown in Supporting Information Figure S1. The mapping of Mn in Supporting Information Figure S1b exhibited similar intensity distribution for boron in Supporting Information Figure S1c, demonstrating the homogeneity of LMB-NBs. Additionally, Supporting Information Figure S1d shows the presence of homogeneously distributed carbon on the surface of the nanobeads. The amount of carbon presented on LMB-NBs was calculated using TGA analysis (Supporting Information Figure S2a), which was about 2.37%. The Raman spectrum in Supporting Information Figure S2b displayed a G-band at 1596 cm^{-1} that originated from ordered graphitized carbon and a D-band at 1347 cm^{-1} related to the breathing mode of k-point phonons of A1g symmetry, confirming the presence of residual carbon on LMB-NBs.

Furthermore, the selected area electron diffraction (SAED) pattern of LMB-NBs (Figure 2b) showed bright spots, which could be indexed via the interplanar spacings according to the monoclinic structure exhibited by LMB-NBs.[19] The TEM image of PANI nanofibers in Figure 2c showed the formation of abundant nanofibers having 50 nm diameter and about 500 nm length. It can also be seen from the TEM of PANI that the nanofibers had uniform size and distribution. The agglomerates observed for PANI in Figure 2c are due to the overlap of nanofibers. In addition, the high-resolution TEM image of PANI (inset in Figure 2c) also supported the formation of fiberlike morphology through chemical copolymerization process. Besides, these fibers were linked together, resulting in the development of the porous PANI networks, which is essential for displaying better electrochemical performance.[33] The fabrication of PANI with controlled diameter and uniformity is important to obtain high-quality products for different potential applications including Li-HCs.[28] It was also reported that the more uniform and thinner PANI nanofibers should have exhibited better performance as compared to nonuniform and thicker nanofibers.[33] The BET surface area of prepared LMB-NBs and PANI nanofibers was calculated to be about 11 and 63 $m^2\ g^{-1}$, respectively, and the corresponding N_2

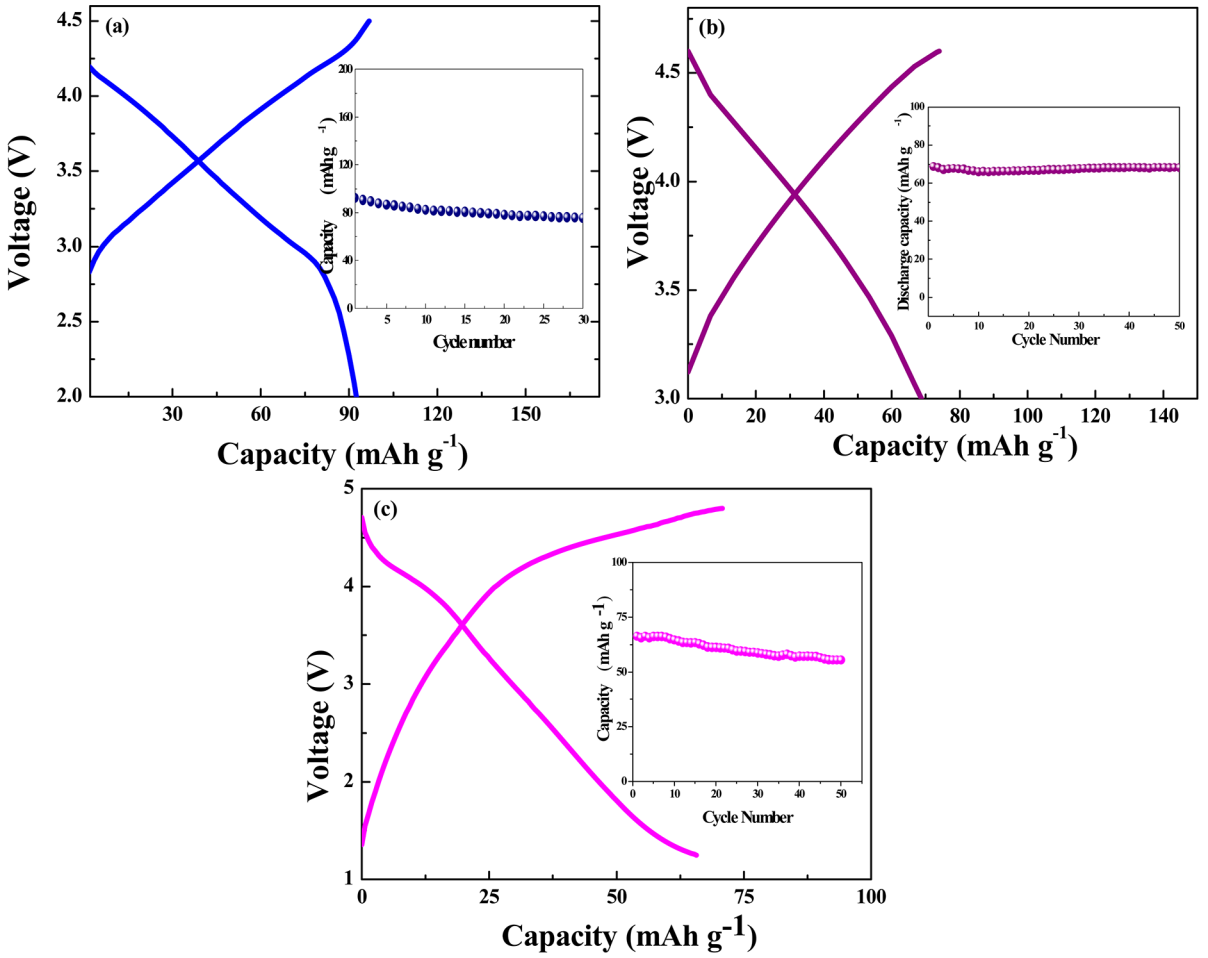

Figure 3. Electrochemical half-cell characterization of (a) Li^+/PANI cell within the potential range of 2−4.5 V, (b) Li^+/AC between 3 and 4.6 V, and (c) Li^+/LMB-NB cell between 1.25 and 4.8 V at 50 mA g^{-1} current density.

adsorption isotherms were illustrated in Supporting Information Figure S3. The PANI nanofibers showed type I isotherm, while LMB-NBs exhibited a distinct hysteresis loop at the relative pressure P/P_0 between 0.4 and 1.0, attributing to type IV with a type H3 hysteresis loop, demonstrating the formation of mesoporous structure. Such a unique feature results in numerous open channels for electrolyte access and facilitates the ultrafast diffusion of ions during the cycling processes at high current rates. The pore size distribution curves of LMB-NB and PANI nanofibers calculated using BJH analysis were given in Supporting Information Figure S3c and S3d, respectively. The BJH curves confirmed the formation of porous structure, which is a desirable feature for effective ion transportation during the C/DC process.

Half-Cell Characterizations. The C−DC characteristics of individual PANI, AC, and LMB-NB electrodes are shown in Figure 3. Figure 3a illustrated the initial C−DC curve of Li^+/PANI cell within the potential range of 2−4.5 V at the current density of 50 mA g^{-1}. PANI exhibited a reversible capacity of 93 mAh g^{-1} in the potential range of 2−4.5 V vs Li, maintaining ∼82% of its initial value after 30 cycles with Coulombic efficiency of more than 98%. It is well-known that the storage mechanism of PANI is mainly based on the doping and undoping of electrolyte active species.[34] The shape of the C−DC curve and obtained discharge capacity were in good agreement with the one proposed by Venancio et al. for PANI film electrodes.[35] The C−DC of Li^+/AC cell exhibited the characteristic of non-Faradaic storage mechanism along with the adsorption/desorption of PF_6^- anion on the surface of AC electrode, which leads to the formation of double layer at the electrode−electrolyte interface.[17] As shown in Figure 3b, the discharge capacity of 68 mAh g^{-1} could be obtained from Li^+/AC cell within a potential range of 3−4.6 V at 50 mA g^{-1} current. The Li^+/AC cell also had excellent cyclability without any capacity fading up to 50 cycles. The prolonged cycling behavior of both AC and PANI clearly revealed that they could be applied as electroactive materials for Li-HCs applications.

The electrochemical half-cell performance of LMB-NB electrode was measured against Li metal anode in 1 M $LiPF_6$ electrolyte at room temperature. Figure 3c showed the initial C−DC curve of Li^+/LMB-NB half-cell within 4.8 and 1.25 V at 50 mA g^{-1} (corresponding to 0.6 C, measured on the basis of the discharge time of LMB-NB electrode) current density. At a lower current rate of 0.6 C, the Li^+/LMB-NB half-cell delivered initial charge and discharge capacities of about 71 and 66 mAh g^{-1}, respectively. The cyclic performance of Li^+/LMB-NB cell (shown as inset in Figure 3a) revealed that ∼84% of capacity was retained after 50 cycle at 0.6 C rate. Moreover, the Li^+/LMB-NB cell also displayed excellent rate performance as presented in Supporting Information Figure S4. Even when the current rate is increased to 4 C, Li^+/LMB-NB cell can still deliver the discharge capacity of ∼55 mAh g^{-1} with 91% of capacity retention after 50 C−DC cycles. Although the initial discharge capacity was eventually decreased with increase in

dx.doi.org/10.1021/am5019034 | ACS Appl. Mater. Interfaces 2014, 6, 11357−11367

current density, the observed electrochemical performance in the present study was much better than that of other reports for monoclinic Li^+/LMB cells.[19,20,30,36,37]

The improved electrochemical performance of LMB-NBs could be attributed to the presence of uniform carbon network between the nanobeads and the reduced particle size of the electrode material. In our present investigation, the homogeneous network formed between the LMB-NBs and amorphous carbon is likely to facilitate lithium ion transport, reduce the polarization, and thus increase the overall electrochemical performance of LMB-NBs. However, LMB-NBs still lack in delivering higher capacity and rate performance over full operating potential range (4.8−1.25 V) due to their poor inherent electronic conductivity, limiting their adoption in commercial LIB application.[20,30]

It is well-known that LMB is a poor electronic conductor. Hence, the focus has been made to study the electrochemical performance of LMB as anode material for LIB by Ma et al.[38] They also proposed that the excess capacity obtained from LMB anode (the theoretical capacity of LMB is 222 mAh g^{-1}) could be attributed to possible formation of new lithiation products. In their study, hexagonal LMB anode showed a discharge capacity of ∼354 mAh g^{-1} at the current density of 50 mA g^{-1} (consumption of 1.6 mol of Li per mol of LMB) with the reversible capacity retention of about 81% after 20 cycles. To compare the anodic performance of LMB-NB with hexagonal LMB, LMB-NB/Li^+ cell was fabricated, and their performance was studied within 0−3 V. The LMB-NB anode delivered a discharge capacity of 357 mAh g^{-1} at 60 mA g^{-1} current density with the reversible capacity retention of about 98% after 50 cycles (Supporting Information Figure S5), suggesting that the structure of LMB-NB as an anode is almost retainable upon continuous C−DC cycling progress.

Considering this phenomenon, a novel approach had been made to utilize LMB-NB as inexpensive high performance anode material in Li-HC configuration along with either PANI or AC as cathode material in 1 M $LiPF_6$ electrolyte. Because the electrochemical capacitive nature of Li-HCs is mainly related to the weight ratio of the individual electrode, the mass balance for fabricating PANI/LMB-NB and AC/LMB-NB cells was optimized from the C−DC performance of individual electrodes vs Li/Li^+ at 50 mA g^{-1} current density.[17,39] On the basis of the results obtained from Figure 3, the optimized mass ratio of cathode to anode for constructing PANI/LMB-NB and AC/LMB-NB was about 1.4:1 and 1:1, respectively. It is well-known that all of the electrodes (PANI, AC, and LMB-NB) got polarized in the positive and negative directions and started acting as the electrode materials in Li-HC configuration.[17]

Characterization of Li-HCs Cells. Figure 4 showed the EIS spectra of PANI/LMB-NB and AC/LMB-NB Li-HC cells recorded between 100 kHz and 100 mHz at open circuit voltage. As expected, both spectra showed a semicircle and an inclined line at low and high frequency regions, respectively. The EIS spectra were fitted according to the equivalent circuit given in the inset of Figure 4. The low frequency semicircle is associated with the Li^+ ion migration resistance (R_s) through the electrode−electrolyte interfacial film; the intermediate frequency semicircle is attributed to the charge transfer resistance (R_{ct}) in the cathode−electrolyte interface, and the line inclined to the real axis corresponds to diffusion of Li^+ into the bulk of the electrode material. The semicircles in the low frequency region are broad and depressed, due to the overlap of the two separate semicircles. As seen from Nyquist plots of Li-HC cells, PANI/LMB-NB cell showed a much lower R_{ct} value of 15 Ω than that of AC/LMB-NB cell (20.27 Ω) due to the better conductive nature of PANI than AC.[34] It is worth mentioning here that the cell with lower R_{ct} value would have exhibited excellent electrochemical capacitive performance.

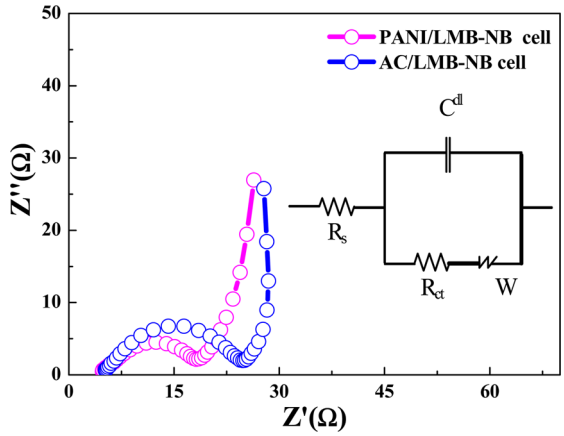

Figure 4. Nyquist plots of freshly made PANI/LMB-NB and AC/LMB-NB Li-HC cells under open circuit voltage conditions. Inset: Equivalent circuit model used for fitting.

Because lowering the resistance directly increases the current flow on the surface of the electrodes, hence significant enhancement in capacitive performance could be expected from PANI/LMB-NB cell.[7,17,34]

The CV studies of the Li-HC cells were conducted at different scan rates in 1 M $LiPF_6$ electrolyte between 0 and 3 V. Figure 5a presented the comparison of CV curves of PANI/LMB-NB and AC/LMB-NB cells, which showed typical rectangular shape even at high scan rate of 50 mV s^{-1} with mirror image approximately, demonstrating excellent capacitive behavior of the cells. Moreover, the PANI/LMB-NB cell delivered apparently a larger area surrounded by CV curves than that of AC/LMB-NB cell, indicating higher electrochemical reversibility of the Li-HC cell based on LMB-NB anode and PANI nanofibers cathode, resulting from the unique morphological feature of LMB-NB as well as from the porous and conductive nature of PANI nanofibers. Moreover, weblike highly interconnected LMB-NBs and uniform formation of thinner PANI nanofibers provided good contact between current collectors, which also aided the performance. Supporting Information Figure S6 illustrated the CV curves of Li-HCs at different scan rates between 0 and 3 V, demonstrating a negative impact of the scan rates on capacitance of the Li-HC cells during potential cycling. Although the shape of the CV curves comparatively changed when the scan rate was increased, all of the curves still showed ideal rectangular behavior, which indicated the high capacitive performance of the cells. However, PANI/LMB-NB cell exhibited enhanced electrochemical characteristics at higher scan rates than that of AC/LMB-NB cell as presented in Supporting Information Figure S6, resulting from the presence of highly conductive emeraldine salt of PANI cathode and the different storage mechanism of PANI/LMB-NB cell. Despite having the same storage mechanism for LMB-NB anodes that are based on electron transfer and intercalation/deintercalation of Li^+ into the LMB-NB structure, the highly reversible doping/dedoping process of PANI cathode enhanced the electrochemical performance of PANI/LMB-NB cell more than the corresponding non-Faradaic storage mechanism, that is, the

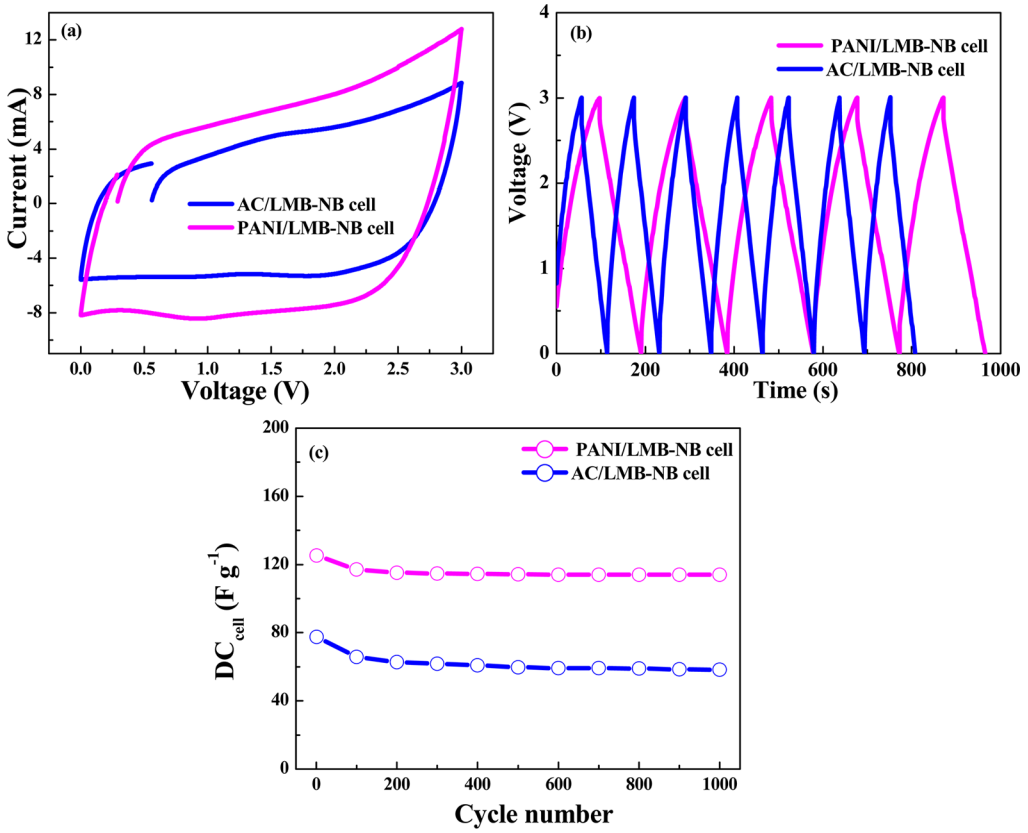

Figure 5. (a) CV traces of Li-HC cells recorded at 50 mV s^{-1} scan rate between 0 and 3 V, (b) C−DC curves, and (c) cyclic performances of Li-HC cells measured at 1 A g^{-1} current density.

adsorption/desorption of PF_6^- anion on the surface of AC cathode in AC/LMB-NB cell.[17,27,34,39−41]

To determine the possible potential application of LMB-NB as high performance anode materials for Li-HC application along with either PANI or AC cathode, the galvanostatic C−DC measurements were carried out within a potential range of 0−3 V at different current rates. The C−DC curves of Li-HC cells at 1 A g^{-1} between 0 and 3 V in 1 M $LiPF_6$ electrolyte are shown in Figure 5b. As seen from Figure 5b, a nonlinear behavior is observed from PANI/LMB-NB and AC/LMB-NB cells during the C−DC process.

Also, the C−DC curves of the hybrid cells were almost symmetrical with a slight curvature nature, which clearly demonstrated that the charge storage mechanism of Li-HC cells was mainly based on the combination of both battery and EDLC-type behavior.[17,39] The electrochemical parameters of the Li-HC cells like discharge capacitance (DC_{cell}), energy density (ED_{cell}), and power density (PD_{cell}) were calculated using the formulas described elsewhere.[16,17,27,29,39,42,43] The internal resistance (IR) of the Li-HC cells was calculated using the following formula:

$$IR = V_{charge} - V_{discharge}/2I \quad (1)$$

where V_{charge} and $V_{discharge}$ are the potentials at the end of charging and at the beginning of discharging, respectively, and I is the applied current density. It is worth mentioning here that decreasing IR value is directly increasing the current flow on the electrode surface, ensuring more lithium ion diffusion toward the electrode, thereby remarkably enhancing the cycling behavior even at high current rates.

A DC_{cell} of about 125 and 77 F g^{-1} was obtained from PANI/LMB-NB and AC/LMB-NB cells, respectively, at 1 A g^{-1} current density. It could also be noted from Figure 5b that the charge and discharge times of both of the cells are almost the same, indicating almost 100% columbic efficiency. In addition, the PANI/LMB-NB cell showed ∼91% of capacitance retention of its initial value at 1 A g^{-1} current density after 1000 C−DC cycles (Figure 5c), whereas the AC/LMB-NB cell had ∼76% cycle life at same C−DC condition. This improved electrochemical performance of the PANI/LMB-NB cell arose due to the morphological feature of both anode and cathode, high pseudocapacitance property of PANI, and the inherent conductivity nature of the electrode materials as shown in Figure 4. Furthermore, the DC_{cell} value achieved in the present investigation for PANI/LMB-NB cell is noteworthy. The capacitance obtained for PANI/LMB-NB cell at 1 A g^{-1} current density in standard organic electrolyte is the highest ever reported value for Li-HCs containing various lithium intercalation electrodes along with excellent cycle life.[8,9,13−17,29,39,41,44−50]

The rate performance of the Li-HC cells was also performed using galvanostatic C−DC studies, and their corresponding plot of DC_{cell} versus current density is given in Figure 6a. As seen from Figure 6a, the DC_{cell} decreased linearly with increasing current rates due to the polarization effect and surface adsorption process in which the ions approached only the outer surface of the electrode material at high current rates, thus predominantly decreasing the active species participating in electrochemical reaction, and hence the low capacitance value was obtained at high C−DC rates.[17,29,39]

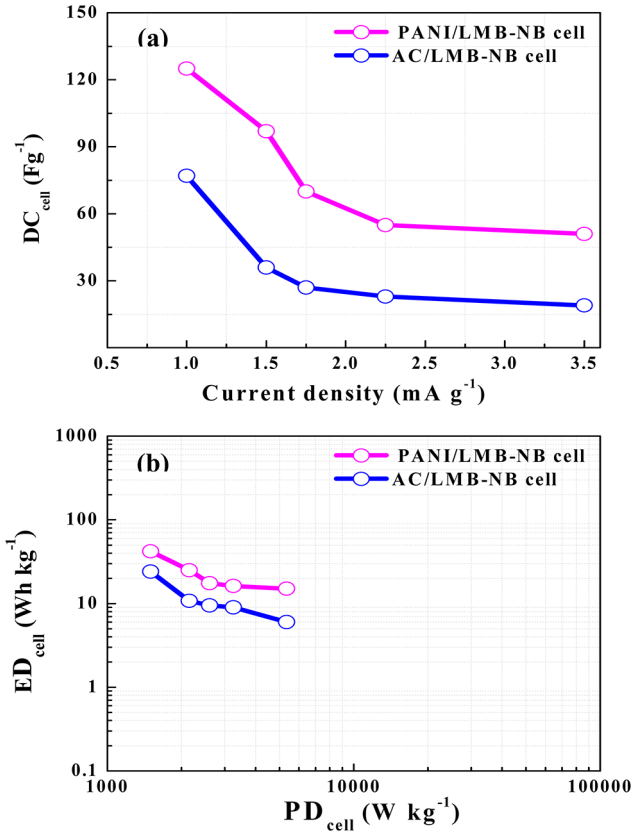

Figure 6. (a) DC_{cell} versus current density and (b) Ragone's plot of Li-HCs in 1 M $LiPF_6$/EC:DMC electrolyte.

At the current density of 1 A g^{-1}, the PANI/LMB-NB cell delivered a DC_{cell} of 125 F g^{-1}, and still maintained about 51 F g^{-1} when the current rate was increased to 3.5 A g^{-1}, while the AC/LMB-NB cell had DC_{cell} of 18 F g^{-1} at a high current rate of 3.5 A g^{-1}. This improved capacitive behavior of PANI/LMB-NB cell could be attributed to its high conductive nature as confirmed in EIS studies in Figure 4, low IR values, and high crystalline nature of LMB-NB, because all of these properties facilitate Li^+ diffusion at high current rates.[17−51] When the current density is increased to 3.5 A g^{-1}, the PANI/LMB-NB and AC/LMB-NB cells had the IR of about 17 and 47 Ω, respectively, indicating high current flow on the surface of the PANI and LMB-NB electrodes, and hence increased rate performance was observed for PANI/LMB-NB cell.[7,17]

Figure 6b presented Ragone's plot of Li-HCs as a function of ED_{cell} and PD_{cell} calculated from C−DC studies at different current rates. It can be seen from the Ragone plots that the PANI/LMB-NB cell showed much higher energy storage characteristics as compared to the AC/LMB-NB cell. In the case of the PANI/LMB-NB cell, an ED_{cell} of 42 Wh kg^{-1} was obtained at a PD_{cell} of 1500 W kg^{-1}, whereas the AC/LMB-NB cell delivered ED_{cell} of about 28 Wh kg^{-1} at the same PD_{cell}. Although there is a monotonous decrease in ED_{cell} observed while increasing PD_{cell}, the PANI/LMB-NB cell still retained the ED_{cell} of 15 Wh kg^{-1} at a high PD_{cell} of 5350 W kg^{-1}. In contrast, the AC/LMB-NB cell provided an ED_{cell} about 5 Wh kg^{-1} at a PD_{cell} 5350 W kg^{-1}, which is a much lower value than that of Li-HC with PANI cathode and LMB-NB anode. It is obvious that the AC cathode is suffering from low bulk density and low charge storage behavior due to the risk of high surface area Li plating during high current rates, resulting in poor energy storage performance of AC/LMB-NB cell.[22,23] Alternatively, porous and thinner PANI nanofibers and highly crystalline LMB-NB with uniform particle size distribution lead to accommodate more electrolyte within the electrodes, thus enhancing conductivity between the active species, improving the overall conductivity of the cell, and hence the electrochemical reaction kinetics of PANI/LMB-NB cell was remarkably improved.[17,33] Moreover, careful optimization of mass ratio of anode to cathode also contributed to achieve higher ED_{cell} and PD_{cell} values.[17,39,45,46] It is worth mentioning here that the capability of PANI/LMB-NB cell in terms of ED_{cell} delivered is one of the best results ever reported among the Li-HC cells fabricated with other lithium intercalation electrodes. The ED_{cell} versus PD_{cell} comparison of PANI/LMB-NB cell with various Li-HCs fabricated in standard organic electrolyte is plotted in Figure 7a. Figure 7a clearly revealed that the PANI/LMB-NB cell outperformed several Li-HCs containing lithium hosts as active material. Furthermore, the ED_{cell} of PANI/LMB-NB cell was also larger than the AC/AC cell,[5,17,22] PANI/AC hybrid cell as reported by Park et al. (ED_{cell} of 18 Wh kg^{-1} at PD_{cell} of 1250 W kg^{-1}),[27] and also outperformed the prelithiated graphitic electrode (G)/AC cell fabricated by Sivakumar et al.[23]

To apply any electrode material for practical applications, high current rate performance along with high cycling behavior are required, and hence the PANI/LMB-NB cell was cycled at 2.25 A g^{-1} for 30 000 deep cycles. Figure 7b clearly demonstrated the PANI/LMB-NB cell's ability of undergoing prolonged electrochemical cycling at harsh C−DC condition in which the hybrid cell exhibited the DC_{cell} of 55 F g^{-1} at 2.25 A g^{-1} current density along with excellent cyclic stability. The DC_{cell} of the hybrid cell initially dropped by ca. 6% during the first 1000 cycles and then remained almost constant thereafter until 30 000 cycles, which revealed its outstanding cycling performance at high current rates than Li-HCs with various lithium intercalation electrode in nonaqueous electrolyte.[8,9,15−17,26,27,29,39,41−53] It can also be noted from Figure 7b that the hybrid cell showed more than 99.5% of columbic efficiency. This exceptional high rate cycling behavior could result from the morphological feature of LMB-NB and PANI nanofibers. The weblike LMB-NB and porous PANI fibers can accommodate more electrolyte within its structure and also provide flexible structure against inherent mechanical stress during the cycling progress at high current rates.[29] Besides, penetration of more electrolyte into the electrode structure stabilized the electrode−electrolyte interface, which facilitated redox reactions and thereby improved the capacitive properties during prolonged cycling. The high rate performance of PANI/LMB-NB cell could also be attributed to its low IR value and improved conductivity as presented in Figure 4.

CONCLUSION

In this study, a novel 3 V high performance Li-HC cell with LMB-NB nanobead anode and PANI cathode was reported. It was found that the PANI/LMB-NB cell can deliver outstanding capacitive performance as compared to that of AC/LMB-NB cell within a potential range of 0−3 V in 1 M $LiPF_6$ electrolyte. For instance, PANI/LMB-NB cell exhibited a DC_{cell} of 125 F g^{-1} at 1 A g^{-1} current density and showed 91% of capacitance retention after 1000 cycles, whereas AC/LMB-NB cell has 77 F g^{-1} capacitance with 76% cycle life. Furthermore, PANI/LMB-NB cell also delivered improved rate performance with more than 99.5% columbic efficiency even after 30 000 cycles. This

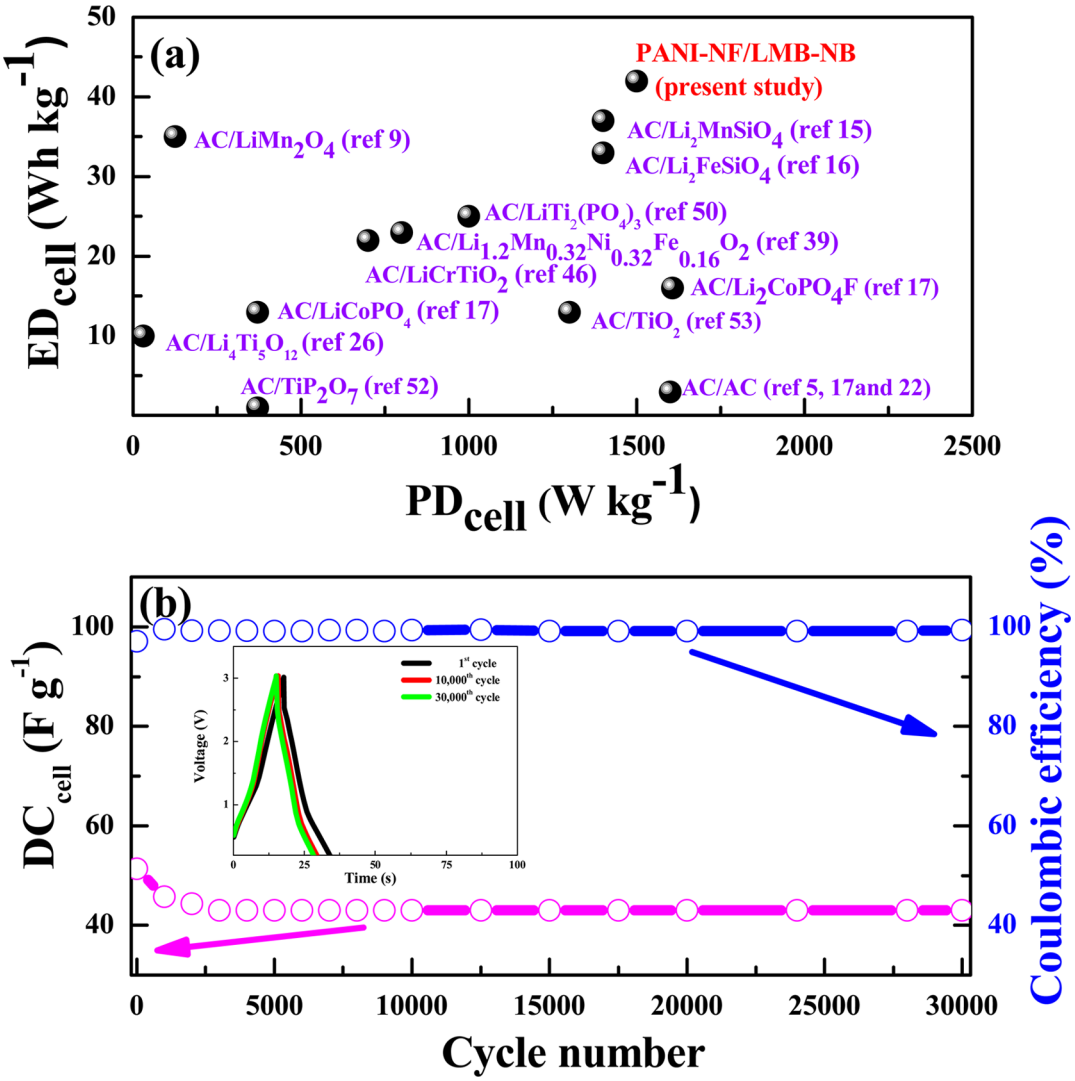

Figure 7. (a) Comparison of ED and PD of different Li-HCs with PANI/LMB-NB cell and (b) cyclic performance of PANI/LMB-NB Li-HC cell at 2.25 A g^{-1} current density for 30 000 deep cycles. Inset showed 1st, 10 000th, and 30 000th C–DC curves of PANI/LMB-NB cell.

outstanding cyclic performance at high current rates could result from its high conductive nature of the PANI/LMB-NB cell and low IR value. Also, the morphological feature of the electrode materials aided the performance, which allowed storing more electrolyte, providing flexible structure against the volume change occurred during the electrochemical reaction and thus improved the structural stability of the electrode materials at high current rate cycling process.

■ ASSOCIATED CONTENT

Supporting Information

EDX, TGA, Raman spectra, and N_2 adsorption/distortion and pore size distribution of the samples. Electrochemical analysis such as CV and C/DC studies of the single electrodes and Li-HCs. This material is available free of charge via the Internet at http://pubs.acs.org.

■ AUTHOR INFORMATION

Corresponding Authors

*Tel.: (226) 700-7583. E-mail: kkaliyap@uwo.ca.
*Tel./fax: +82 62 530 1904. E-mail: leeys@chonnam.ac.kr.

Notes

The authors declare no competing financial interest.

■ REFERENCES

(1) Kotz, R.; Carlen, M. Principles and Applications of Electrochemical Capacitors. *Electrochim. Acta* **2000**, *45*, 2483–2498.
(2) Zhao, X.; Sanchez, B. M.; Dobson, P. J.; Grant, P. S. The Role of Nanomaterials in Redox-based Supercapacitors for Next Generation Energy Storage Devices. *Nanoscale* **2011**, *3*, 839–855.
(3) Brousse, T.; Toupin, M.; Belanger, D. A Hybrid Activated Carbon-Manganese Dioxide Capacitor Using a Mild Aqueous Electrolyte. *J. Electrochem. Soc.* **2004**, *151*, A614–A622.
(4) Xue, Y.; Chen, Y.; Zhang, M. L.; Yan, Y. D. A New Asymmetric Supercapacitor Based on λ-MnO2 and Activated Carbon Electrodes. *Mater. Lett.* **2008**, *62*, 3884–3886.
(5) Simon, P.; Gogotsi, Y. Materials for Electrochemical Capacitors. *Nat. Mater.* **2008**, *7*, 845–854.
(6) Chen, Z.; Augustyn, V.; Wen, J.; Zhang, Y.; Shen, M.; Dunn, B.; Lu, Y. High-Performance Supercapacitors Based on Intertwined CNT/V_2O_5 Nanowire Nanocomposites. *Adv. Mater.* **2011**, *23*, 791–795.
(7) Karthikeyan, K.; Amaresh, S.; Kalpana, D.; KalaiSelvan, R.; Lee, Y. S. Electrochemical Supercapacitor Studies of Hierarchical Structured Co^{2+}-substituted SnO_2 Nanoparticles by a Hydrothermal Method. *J. Phys. Chem. Solids* **2012**, *73*, 363–367.

(8) Pasquier, A. D.; Plitz, I.; Gural, J.; Badway, F.; Amatucci, G. G. Power-ion Battery: Bridging the Gap between Li-Ion and Supercapacitor Chemistries. *J. Power Sources* **2004**, *136*, 160−170.
(9) Wang, Y. G.; Xia, Y. A New Concept Hybrid Electrochemical Surpercapacitor: Carbon/$LiMn_2O_4$ Aqueous System. *Electrochem. Commun.* **2005**, *7*, 1138−1142.
(10) Amatucci, G. G.; Badway, F.; Pasquier, A. D.; Zheng, T. An Asymmetric Hybrid Nonaqueous Energy Storage Cell. *J. Electrochem. Soc.* **2001**, *148*, A930−A939.
(11) Wang, Y. G.; Xia, Y. Y. Hybrid Aqueous Energy Storage Cells Using Activated Carbon and Lithium-Intercalated Compounds I. The C/$LiMn_2O_4$ System. *J. Electrochem. Soc.* **2006**, *153*, A450−A454.
(12) Wang, Y.; Luo, C.; Wang, C. X.; Xia, Y. Hybrid Aqueous Energy Storage Cells Using Activated Carbon and Lithium-Ion Intercalated Compounds II. Comparison of $LiMn_2O_4$, $LiCo_{1/3}Ni_{1/3}Mn_{1/3}O_2$, and $LiCoO_2$ Positive Electrodes. *J. Electrochem. Soc.* **2006**, *153*, A1425−A1431.
(13) Vasanthi, R.; Kalpana, D.; Renganathan, N. G. Olivine-type Nanoparticle for Hybrid Supercapacitors. *J. Solid State Electrochem.* **2007**, *12*, 961−969.
(14) Hu, X. B.; Huai, Y. J.; Lin, Z. J.; Suo, J. S.; Deng, Z. H. A ($LiFePO_4$ − AC)/$Li_4Ti_5O_{12}$ Hybrid Battery Capacitor. *J. Electrochem. Soc.* **2007**, *154*, A1026−A1030.
(15) Karthikeyan, K.; Aravindan, V.; Lee, S. B.; Jang, I. C.; Lim, H. H.; Park, G. J.; Yoshio, M.; Lee, Y. S. Electrochemical Performance of Carbon-coated Lithium Manganese Silicate for Asymmetric Hybrid Supercapacitors. *J. Power Sources* **2010**, *195*, 3761−3764.
(16) Karthikeyan, K.; Aravindan, V.; Lee, S. B.; Jang, I. C.; Lim, H. H.; Park, G. J.; Yoshio, M.; Lee, Y. S. A Novel Asymmetric Hybrid Supercapacitor Based on Li_2FeSiO_4 and Activated Carbon Electrodes. *J. Alloys Compd.* **2010**, *504*, 224−227.
(17) Karthikeyan, K.; Amaresh, S.; Kim, K. J.; Kim, S. H.; Chung, K. Y.; Cho, B. W.; Lee, Y. S. A High Performance Hybrid Capacitor with Li_2CoPO_4F Cathode and Activated Carbon Anode. *Nanoscale* **2013**, *5*, 5958−5964.
(18) Legagneur, V.; An, Y.; Mosbah, A.; Portal, R.; Salle, A. L. G. L.; Verbaere, A.; Guyomard, D.; Piffard, Y. LiMBO3 (M= Mn, Fe, Co) Synthesis, Crystal Structure and Lithium Deinsertion/Insertion Properties. *Solid State Ionics* **2001**, *139*, 37−46.
(19) Afyon, S.; Kundu, D.; Krumeich, F.; Nesper, R. Nano $LiMnBO_3$, a High-Capacity Cathode Material for Li-ion Batteries. *J. Power Sources* **2013**, *224*, 145−151.
(20) Kim, J. C.; Moore, C. J.; Kang, B.; Hautier, G.; Jain, A.; Ceder, G. Synthesis and Electrochemical Properties of Monoclinic $LiMnBO_3$ as a Li Intercalation Material. *J. Electrochem. Soc.* **2011**, *158*, A309−A315.
(21) Aravindan, V.; Karthikeyan, K.; Amaresh, S.; Lee, Y. S. $LiMnBO_3$/C: A Potential Cathode Material for Lithium Batteries. *Bull. Korean Chem. Soc.* **2010**, *31*, 1506−1508.
(22) Frackowiaka, E.; Béguinb, F. Carbon Materials for the Electrochemical Storage of Energy in Capacitors. *Carbon* **2001**, *39*, 937−950.
(23) Sivakkumar, S. R.; Pandolfo, A. G. Evaluation of Lithium-Ion Capacitors Assembled with Pre-Lithiated Graphite Anode and Activated Carbon Cathode. *Electrochim. Acta* **2012**, *65*, 280−287.
(24) Snook, G. A.; Kao, P.; Best, A. S. Conducting-Polymer-Based Supercapacitor Devices and Electrodes. *J. Power Sources* **2011**, *196*, 1−12.
(25) Laforgue, A.; Simon, P.; Fauvarque, J. F.; Mastragostino, M.; Soavi, F.; Sarrau, J. F.; Lailler, P.; Conte, M.; Rossi, E.; Saguattie, S. Activated Carbon/Conducting Polymer Hybrid Supercapacitors. *J. Electrochem. Soc.* **2003**, *150*, A645−A651.
(26) Pasquier, A. D.; Laforgue, A.; Simon, P. $Li_4Ti_5O_{12}$/Poly-(methyl)thiophene Asymmetric Hybrid Electrochemical Device. *J. Power Sources* **2004**, *125*, 95−102.
(27) Park, J. H.; Park, O. O. Hybrid Electrochemical Capacitors Based on Polyaniline and Activated Carbon Electrodes. *J. Power Sources* **2002**, *111*, 185−190.
(28) Ramya, R.; Sivasubramanian, R.; Sangaranarayanan, M. V. Conducting Polymers-Based Electrochemical Supercapacitors - Progress and Prospects. *Electrochim. Acta* **2013**, *101*, 109−129.
(29) Karthikeyan, K.; Amaresh, S.; Aravindan, V.; Kim, H.; Kang, K. S.; Lee, Y. S. Unveiling Organic−Inorganic Hybrids as a Cathode Material for High Performance Lithium-Ion Capacitors. *J. Mater. Chem. A* **2013**, *1*, 707−714.
(30) Li, S.; Xu, L.; Li, G.; Wang, M.; Zhai, Y. In-situ Controllable Synthesis And Performance Investigation of Carbon-Coated Monoclinic and Hexagonal LiMnBO3 Composites as Cathode Materials in Lithium-Ion Batteries. *J. Power Sources* **2013**, *236*, 54−60.
(31) Pawlak, L.; Falkowski, K.; Pokrzywnicki, S. The Influence of Cation Arrangement on the EPR Spectrum of Mn^{2+} in the Spinel Compounds CdB_2X_4. *J. Solid State Chem.* **1981**, *37*, 228−231.
(32) Furukawa, Y.; Ueda; Hyodo, Y.; Harada, I.; Nakajima, T.; Kawagoe, T. Determination of Crosslink Density in Thermoset Polymers by Use of Solid-State Proton NMR Techniques. *Macromolecules* **1988**, *21*, 1292−1297.
(33) Huang, J. Syntheses and Applications of Conducting Polymer Polyaniline Nanofibers. *Pure Appl. Chem.* **2006**, *78*, 15−27.
(34) Nova, P.; Muller, K.; Santhanam, K.; Haas, O. Electrochemically Active Polymers for Rechargeable Batteries. *Chem. Rev.* **1997**, *97*, 207−281.
(35) Venancio, E. C.; Motheo, A. J.; Amaral, F. A.; Bocchi, N. Performance of Polyaniline Electrosynthesized in the Presence of Trichloroacetic Acid as a Battery Cathode. *J. Power Sources* **2001**, *94*, 36−39.
(36) Yamada, A.N.; Iwane, A. J.; Nishimura, S.; Koyama, Y.; Tanaka, I. Synthesis and Electrochemistry of Monoclinic $Li(Mn_xFe_{1-x})BO_3$: A Combined Experimental and Computational Study. *J. Mater. Chem.* **2011**, *21*, 10690−10696.
(37) Lee, K. J.; Lee, S. K.; Uhma, S.; Yoon, J. S.; Kim, D. W.; Hong, H. S. Synthesis and Characterization of $LiMnBO_3$ Cathode Material For Lithium Ion Batteries. *Curr. Appl. Phys.* **2013**, *13*, 1440−1443.
(38) Ma, R.; Shao, L.; Wu, K.; Lao, M.; Shui, M.; Chen, C.; Wang, D.; Long, N.; Ren, Y.; Shu, J. Electrochemical Behaviors of Hexagonal LiMnBO3 as Lithium Storage Host Material for Lithium-Ion Batteries. *Ceram. Int.* **2013**, *39*, 9309−9317.
(39) Karthikeyan, K.; Kim, S. H.; Kim, K. J.; Lee, S. N.; Lee, Y. S. Low Cost, Eco-Friendly Layered $Li1_{.2}(Mn_{0.32}Ni_{0.32}Fe_{0.16})O_2$ Nanoparticles for Hybrid Supercapacitor Applications. *Electrochim. Acta* **2013**, *109*, 595−601.
(40) Zou, W.; Wang, W.; He, B.; Sun, M.; Yin, Y. Supercapacitive Properties of Hybrid Films Oo Manganese Dioxide and Polyaniline Based an Active Carbon in Organic Electrolyte. *J. Power Sources* **2010**, *21*, 7489−7493.
(41) Zhang, K.; Zhang, L. L.; Zhao, X. S.; Wu, J. Graphene/Polyaniline Nanofiber Composites as Supercapacitor Electrodes. *Chem. Mater.* **2010**, *22*, 1392−1401.
(42) Zhu, Y.; Murali, S.; Stoller, M. D.; Ganesh, K. J.; Cai, W.; Ferreira, P. J.; Pirkle, A.; Wallace, R. M.; Cychosz, K. A.; Thommes, M.; Su, D.; Stach, E. A.; Ruoff, R. S. Carbon-Based Supercapacitors Produced by Activation of Graphene. *Science* **2011**, *332*, 1537−1541.
(43) Stoller, M. D.; Ruoff, R. S. Best Practice Methods for Determining an Electrode Material's Performance for Ultracapacitors. *Energy Environ. Sci.* **2010**, *3*, 1294−1301.
(44) Naoi, K.; Simon, P. New Materials and New Confgurations for Advanced Electrochemical Capacitors. *Electrochem. Soc. Interface* **2008**, *17*, 34−37.
(45) Aravindan, V.; Chuiling, W.; Reddy, M. V.; Rao, G. V. S.; Chowdari, B. V. R.; Madhavi, S. Carbon Coated Nano-$LiTi_2(PO_4)_3$ Electrodes for Non-Aqueous Hybrid Supercapacitors. *Phys. Chem. Chem. Phys.* **2012**, *14*, 5808−5814.
(46) Aravindan, V.; Chuiling, W.; Madhavi, S. High Power Lithium-Ion Hybrid Electrochemical Capacitors Using Spinel $LiCrTiO_4$ as Insertion Electrode. *J. Mater. Chem.* **2012**, *22*, 16026−16031.
(47) Aravindan, V.; Cheah, Y. L.; Wee, G.; Chowdari, B. V. R.; Madhavi, S. Fabrication of High Energy-Density Hybrid Super-

capacitors Using Electrospun V_2O_5 Nanofibers with a Self-Supported Carbon Nanotube Network. *ChemPlusChem* **2012**, *77*, 570−575.
(48) Ma, S. B.; Nam, K. W.; Yoon, S. B.; Yang, X. Q.; Ahn, K. Y.; Oh, K. H.; Kim, K. B. A Novel Concept of Hybrid Capacitor Based on Manganese Oxide Materials. *Electrochem. Commun.* **2007**, *9*, 2807−2811.
(49) Hua, X.; Denga, Z.; Suo, J.; Pan, Z. A High Rate, High Capacity and Long Life $(LiMn_2O_4+AC)/Li_4Ti_5O_{12}$ Hybrid Battery−Supercapacitor. *J. Power Sources* **2009**, *187*, 635−639.
(50) Luo, J. Y.; Liu, J. L.; He, P.; Xia, Y. Y. A Novel $LiTi_2(PO_4)_3/MnO_2$ Hybrid Supercapacitor in Lithium Sulfate Aqueous Electrolyte. *Electrochim. Acta* **2008**, *53*, 8128−8133.
(51) Wang, Z.; Sun, Y.; Chen, L.; Huang, X. Electrochemical Characterization of Positive Electrode Material $LiNi_{1/3}Co_{1/3}Mn_{1/3}O_2$ and Compatibility with Electrolyte for Lithium-Ion Batteries. *J. Electrochem. Soc.* **2004**, *151*, A914−A921.
(52) Aravindan, V.; Reddy, M. V.; Madhavi, S.; Mhaisalkar, S. G.; Rao, G. V. S.; Chowdari, B. V. R. Hybrid Supercapacitor with Nano-TiP_2O_7 as Intercalation Electrode. *J. Power Sources* **2011**, *196*, 8850−8854.
(53) Wang, Q.; Wen, Z.; Li, J. A Hybrid Supercapacitor Fabricated with a Carbon Nanotube Cathode and a TiO_2-B Nanowire Anode. *Adv. Funct. Mater.* **2006**, *16*, 2141−2146.